Biochemical and Biophysical Research Communications 443 (2014) 635–640

Contents lists available at ScienceDirect

Biochemical and Biophysical Research Communications

journal homepage: www.elsevier.com/locate/ybbrc

Imaging Axl expression in pancreatic and prostate cancer xenografts

Sridhar Nimmagadda [a,b,*,2], Mrudula Pullambhatla [a], Ala Lisok [a], Chaoxin Hu [c,1], Anirban Maitra [b,c,1], Martin G Pomper [a,b,*,2]

[a] Russell H. Morgan Department of Radiology and Radiological Science, Johns Hopkins University, Baltimore, MD 21287, United States
[b] Sidney Kimmel Comprehensive Cancer Center, Johns Hopkins University, Baltimore, MD 21287, United States
[c] Department of Pathology, Johns Hopkins University, Baltimore, MD 21287, United States

ARTICLE INFO

Article history:
Received 28 November 2013
Available online 11 December 2013

Keywords:
Molecular imaging
ImmunoPET
Receptor tyrosine kinase
Axl
Gas6

ABSTRACT

The receptor tyrosine kinase Axl is overexpressed in and leads to patient morbidity and mortality in a variety of cancers. Axl–Gas6 interactions are critical for tumor growth, angiogenesis and metastasis. The goal of this study was to investigate the feasibility of imaging graded levels of Axl expression in tumors using a radiolabeled antibody. We radiolabeled anti-human Axl (Axl mAb) and control IgG1 antibodies with ^{125}I with high specific radioactivity and radiochemical purity, resulting in an immunoreactive fraction suitable for *in vivo* studies. Radiolabeled antibodies were investigated in severe combined immunodeficient mice harboring subcutaneous CFPAC (Axl^{high}) and Panc1 (Axl^{low}) pancreatic cancer xenografts by *ex vivo* biodistribution and imaging. Based on these results, the specificity of [^{125}I]Axl mAb was also validated in mice harboring orthotopic Panc1 or CFPAC tumors and in mice harboring subcutaneous 22Rv1 (Axl^{low}) or DU145 (Axl^{high}) prostate tumors by *ex vivo* biodistribution and imaging studies at 72 h post-injection of the antibody. Both imaging and biodistribution studies demonstrated specific and persistent accumulation of [^{125}I]Axl mAb in Axl^{high} (CFPAC and DU145) expression tumors compared to the Axl^{low} (Panc1 and 22Rv1) expression tumors. Axl expression in these tumors was further confirmed by immunohistochemical studies. No difference in the uptake of radioactivity was observed between the control [^{125}I]IgG1 antibody in the Axl^{high} and Axl^{low} expression tumors. These data demonstrate the feasibility of imaging Axl expression in pancreatic and prostate tumor xenografts.

1. Introduction

Axl is a member of the large receptor tyrosine kinase (RTK) family of transmembrane proteins. Axl belongs to the TAM (tyro-3, Axl and Mer) subfamily of RTKs and consists of a characteristic structure including a two immunoglobin-like domains with dual fibronectin type III repeats in the extracellular component and a cytoplasmic kinase domain [1,2]. Axl is ubiquitously expressed in a wide variety of tissues and cells including the hippocampus and cerebellum, monocytes, macrophages, platelets, endothelial cells, heart, skeletal muscle, liver, kidney, and testis [3]. Axl binds to growth arrest-specific gene 6 (Gas-6) and exerts biological effects through PI3K, STAT and NF-kB signaling pathways [1,2,4].

Axl overexpression and ligand-induced activation are observed in a variety of cancers including breast [5], colon [6], esophageal [7], glioma [8], liver [9], lung [10], thyroid [11], pancreatic [12] and prostate [13,14]. Axl binding to its ligand Gas-6 promotes growth, survival, and proliferation by activation of the RAS/RAF/MAPK/ERK1/2 and PI3K signaling pathways [2]. Axl overexpression increases motility in glioblastoma cells through regulation of the actin cytoskeleton [15]. Similarly, Axl overexpression confers an invasive phenotype to breast cancer cells that could be reduced by RNA interference, suggesting that Axl plays a role in cell motility and adhesion [16]. Furthermore, Axl knockdown completely abolished the ability of cells emerging from primary tumors to colonize the lungs [16]. Supporting these preclinical studies, Axl expression correlates with adherence and metastatic potential of lung cancer cells in patients with adenocarcinoma [10].

Axl overexpression and its role in pathogenesis have been well described for pancreatic and prostate cancers [2,12–14]. Previously we have shown that 55% of pancreatic adenocarcinomas tested were positive for Axl, and that this expression was associated with lymph node metastasis [12]. Tumors with high Axl expression were also associated with a poor survival rate compared to those with low levels of expression [12]. Genetic downregulation of Axl

* Corresponding authors. Address: Johns Hopkins Medical Institutions, 1550 Orleans Street, 491 CRB II, Baltimore, MD 21287, United States. Fax: +1 410 614 3147 (S. Nimmagadda). Fax: +1 443 817 0990 (M. Pomper).
E-mail addresses: snimmag1@jhmi.edu (S. Nimmagadda), mpomper@jhmi.edu (M.G Pomper).
[1] Present address: Department of Pathology, UT MD Anderson Cancer Center, 1515 Holcombe Blvd, Houston, TX 77030, United States.
[2] These authors contributed equally to this work.

0006-291X/$ - see front matter © 2013 Elsevier Inc. All rights reserved.
http://dx.doi.org/10.1016/j.bbrc.2013.12.014

in pancreatic cancer cells resulted in reduced invasive and migratory capacity, demonstrating the importance of Axl in metastasis [12]. Similarly, nearly 50% of prostate tumors were shown to upregulate Axl by 2- to 1500-fold [14]. In prostate tumors the intensity of staining for Axl increases with tumor grade, and bone metastases have elevated expression compared to the metastases to lymph nodes [13].

Because of its role in tumor growth, proliferation and metastasis, Axl is considered a therapeutic target. Several Axl inhibitors, including low-molecular-weight agents and antibodies, have been reported. Axl inhibition, using low-molecular-weight inhibitors or shRNA knockdown, resulted in reduced tumor growth, metastasis and angiogenesis in a variety of tumor models [14,15,17–21]. Recently a Phase I clinical trial of the Axl inhibitor R428 (also known as BGB324) has been initiated [22]. Due to the emerging role of Axl in cancer, we envisioned that the development of a corresponding imaging agent is timely. In proof-of-principle studies, we demonstrate that graded levels of Axl expression could be imaged using a radiolabeled mouse anti-human Axl monoclonal antibody ([^{125}I]Axl mAb) in subcutaneous pancreatic and prostate tumor xenografts and in orthotopic pancreatic tumor xenografts by single photon emission computed tomography/computed tomography (SPECT/CT). Biodistribution studies performed *ex vivo* confirmed the imaging results, which were further validated through immunohistochemistry.

2. Materials and methods

2.1. Cell lines

Cell lines were purchased from ATCC (Manassas, VA). The pancreatic cell lines CFPAC, and Panc1 and the prostate cell lines DU145 and 22Rv1 cell lines were cultured in DMEM and RPMI medium, respectively, supplemented with 10% FBS, penstrep and L-glutamine.

2.2. Antibody radiolabeling

The mouse anti-human Axl antibody (clone 108724) and Isotype matched control mouse IgG_1 antibody (Clone 11711) were purchased from R&D systems, Inc. (Minneapolis, MN). [^{125}I]NaI was purchased from Perkin Elmer (Waltham, MA). Both control and Axl antibodies were radiolabeled by the iodogen method as described previously [23].

2.3. Animal models

Female NOD/SCID mice, six- to eight-weeks-old, weighing between 25 and 30 g were purchased from the Johns Hopkins Immunocompromised Mouse Core. Experimental procedures using animals were conducted according to protocols approved by the Johns Hopkins Animal Care and Use Committee. Mice were implanted subcutaneously (s.c.) with CFPAC, and Panc1 cells (5×10^6 cells/100 μL, 1/1 (v/v) PBS/Matrigel) in the opposite upper flanks. Due to significant differences in tumor growth rates, prostate cell lines DU145 and 22Rv1 (3×10^6 cells/100 μL, 1/1 (v/v) PBS/Matrigel) were inoculated into separate groups of mice. After three to four weeks or when the tumor size was 200–400 mm^3, animals were used for biodistribution and SPECT/CT imaging experiments.

Orthotopic pancreatic tumors were generated as described previously by us [24]. Prior to surgery, s.c. tumors generated as described above were harvested and cut into cubes of ~1 mm^3. Briefly, animals were anesthetized using ketamine/xylazine and the abdomen was opened via a ~1 cm subcostal left incision. After visualization of the spleen and adherent pancreas, a small pocket was prepared inside the pancreas using microscissors into which one piece of the s.c. tumor was implanted and sutured with an 8–0 nylon monofilament suture. The incision and the abdominal wall were sutured with 6–0 nylon monofilament string, and the skin incision was closed using wound clips.

2.4. Data analysis

Statistical analysis was performed using an unpaired, two-tailed *t* test. *P*-values <0.05 for the comparison between tumors that express high and low levels of Axl were considered significant.

Detailed procedures for cell binding and immunoreactivity assays, immunoblotting, SPECT-CT imaging, *ex vivo* biodistribution and immunohistochemistry can be found in Supplementary methods.

3. Results

3.1. Antibody radiolabeling

Radiolabeling of both of the antibodies resulted in greater than 50% yields with 6.3 ± 2.24 and 4.1 ± 1.7 μCi/μg of specific radioactivity for Axl and IgG1 antibodies, respectively. Radiochemical purities were >95% as determined by thin-layer chromatography.

3.2. Axl expression and antibody specificity

Immunoblotting identified Axl expression in the order: DU145 > CFPAC > Panc1 > 22Rv1 (Fig. 1A). As shown in Fig. 1B, [^{125}I]Axl mAb showed high specificity towards Axl^{high} positive DU145, CFPAC and Panc1 cells compared to the Axl^{low} 22Rv1 cells. The immunoreactive fraction (IF) of the radiolabeled antibody was 68.4 ± 16.8% (Fig. 1C).

3.3. SPECT/CT imaging

SPECT/CT imaging of mice harboring CFPAC and Panc1 tumors with [^{125}I]Axl mAb demonstrated a clear and specific accumulation of radioactivity in the CFPAC tumors by 24 h, which could still be clearly visualized at 120 h (Fig. 2A and Supplementary Fig. 1). At early time points the accumulation of radioactivity could be seen in the tumor, liver and heart (Fig. 2A). At 120 h post-injection, the accumulation of radioactivity was observed mostly within tumor and heart. The tumor-to-background contrast was at a maximum at 72 h post-injection of the [^{125}I]Axl mAb.

Based on imaging and biodistribution studies in s.c. pancreatic tumors, we also acquired SPECT/CT imaging in orthotopic CFPAC tumors and prostate tumors at 72 h post-injection of the [^{125}I]Axl mAb. The corresponding SPECT/CT images showed accumulation of radioactivity in the orthotopic CFPAC tumor (Fig. 3A). Similarly, specific accumulation of radioactivity can be seen in the Axl^{high} DU145 (Fig. 4A) tumor compared to the Axl^{low} 22Rv1 tumor (Fig. 4B). Axl expression in tumors was confirmed by staining tumor sections from uninjected mice from the same cohort (Figs. 2B, C, 3C, D and 4D). These studies showed high Axl expression in the CFPAC and DU145 tumors, confirming *in vitro* immunoblot studies of the cell lines and further supporting the specific [^{125}I]Axl mAb accumulation seen in these tumors.

3.4. Ex vivo biodistribution

To quantify the degree of radio-antibody uptake on a per organ basis, tumor-bearing animals were injected with either [^{125}I]Axl

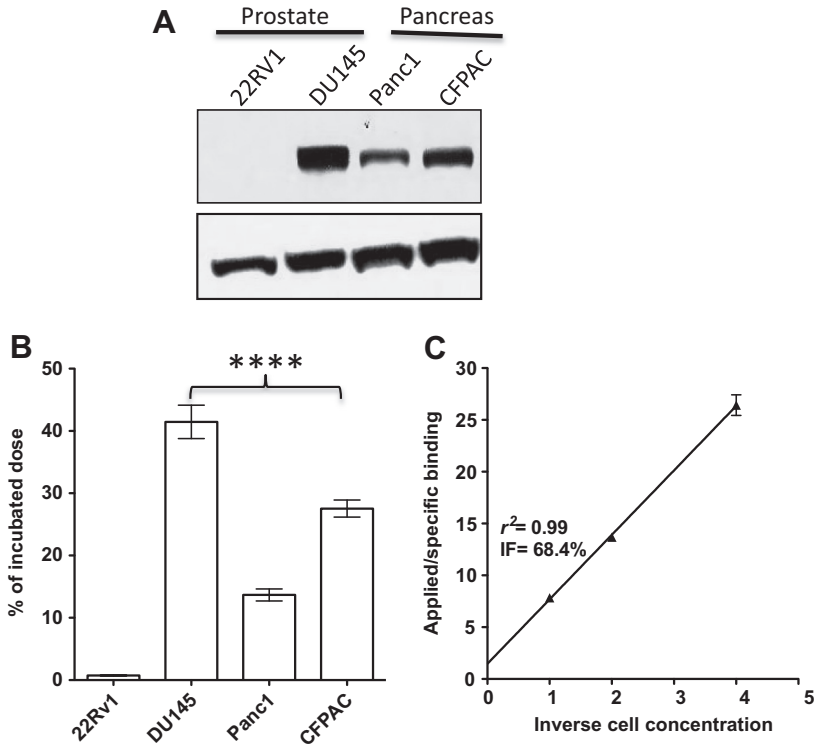

Fig. 1. Axl expression and [^{125}I]Axl mAb binding specificity to Axl. Total Axl expression in CFPAC, Panc1, DU145 and 22Rv1 cells (A). CFPAC, Panc1, DU145 and 22Rv1 cells at 60–70% confluence in 6-well plates were incubated with 1 μCi/mL of [^{125}I]Axl mAb at 4 °C for 30 min. Data are represented as percentage of incubated dose per million cells. A representative graph of mean ± the standard error of the mean (SEM) is shown (B). The significance of the value is indicated by asterisks (∗) and the comparative reference is the 22Rv1 cell line. $^{****}P < 0.0001$. Immunoreactivity plot of [^{125}I]Axl mAb for CFPAC cells (C).

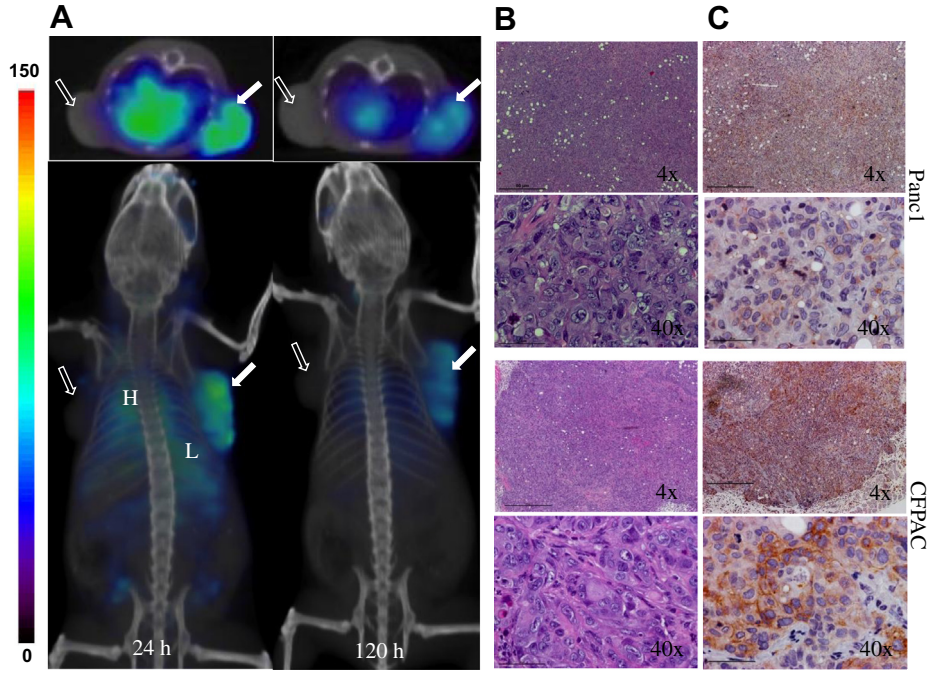

Fig. 2. SPECT/CT images of Axl expression in subcutaneous pancreatic cancer xenografts with [^{125}I]Axl mAb. NOD/SCID mice bearing CFPAC and Panc1 pancreatic xenografts were injected with 0.75 mCi of [^{125}I]Axl mAb via the tail vein. SPECT/CT images were acquired at various time points post-injection of the [^{125}I]Axl mAb. Images were adjusted to the same maximum value. Representative trans-axial and volume-rendered images acquired at 24 and 120 h time points are shown (A). filled arrow, CFPAC tumor; unfilled arrow, Panc1 tumor; H, heart; L, liver. Hematoxylin and eosin (B) and Axl (C) staining of the Panc1 and CFPAC xenografts at 4 and 40× magnification.

mAb or [^{125}I]IgG$_1$ and were followed for five days. Biodistribution results of [^{125}I]Axl mAb in CFPAC and Panc1 tumor-bearing mice at 24, 48, 72, 96 and 136 h post-injection are shown in Supplementary Fig. 2. The [^{125}I]Axl mAb showed consistently

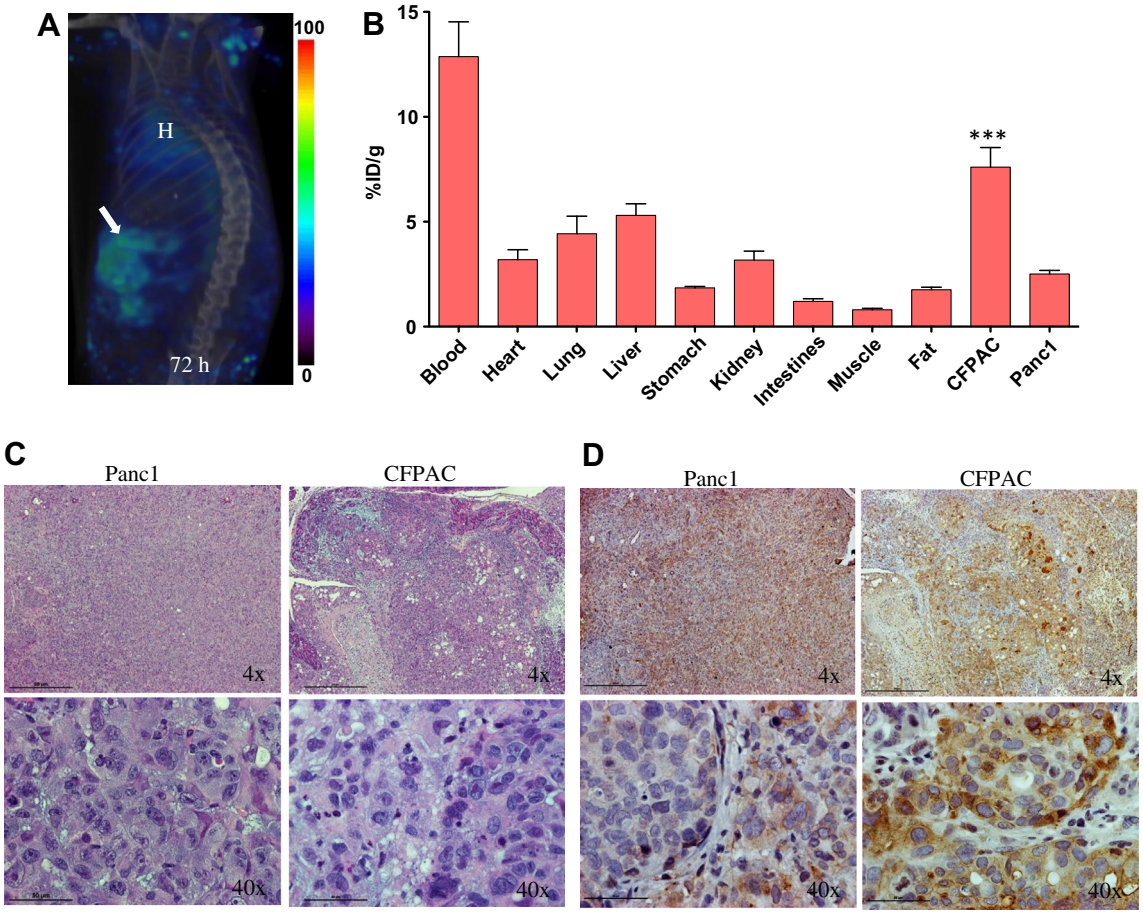

Fig. 3. SPECT/CT imaging and *ex vivo* biodistribution of [^{125}I]Axl mAb in orthotopic pancreatic xenografts. NOD/SCID mice bearing orthotopic CFPAC pancreatic xenografts were given 0.75 mCi of [^{125}I]Axl mAb *via* tail vein injection. SPECT/CT images were acquired at 72 h post-injection of the [^{125}I]Axl mAb. Representative transaxial and volume rendered images are shown (A); filled arrow, tumor; H, heart. NOD/SCID mice harboring CFPAC and Panc1 orthotopic pancreatic xenografts were given 30–35 μCi of [^{125}I]Axl mAb via tail vein injection. At 72 h post-injection, selected tissues and tumors were harvested, weighed and radioactivity was counted in gamma spectrometer. Values were converted into percentage of injected dose per gram of tissue (%ID/g). Data are means ± SEM of three or four animals. The significance of the value is indicated by asterisks (∗) and the comparative reference is uptake to that in the Panc1 tumor. $^{***}P < 0.001$ (B). Hematoxylin and eosin (C) and Axl (D) staining of the Panc1 and CFPAC xenografts at 4 and 40× magnification.

higher tumor uptake in the Axl^{high} CFPAC tumors than in Axl^{low} Panc1 tumors at all time points. The CFPAC to Panc1 ratios were 2.1, 3.8 and 2.0 at 24, 72 and 136 h post-injection, respectively. The tumor-to-muscle ratios (T/M) for CFPAC tumors for the [^{125}I]Axl mAb were 9.1 ± 1.8, 8.4 ± 1.5, 9.7 ± 0.7, 9.9 ± 0.2 and 7.8 ± 1.3 at 24, 48, 72, 96 and 136 h post-injection, respectively. Similarly, the tumor-to-muscle ratios for Panc1 tumors were 3.8 ± 1.2, 3.6 ± 0.2, 2.9 ± 0.3, 3.0 ± 0.3, 3.8 ± 0.7 at 24, 48, 72, 96 and 136 h post-injection, respectively. The tumor-to-blood ratios for both tumors were less than one at all time points. Because of the high target-to-non-target ratios observed at 72 h post-injection in s.c. pancreatic xenografts, biodistribution studies were performed at 72 h after the injection of [^{125}I]Axl mAb in orthotopic pancreatic (Fig. 3B) and s.c. prostate xenografts (Fig. 4C). In the orthotopic tumors, T/M ratios of 6.9 ± 0.8 and 4.0 ± 0.3 were observed for the CFPAC and Panc1 tumors, respectively. The T/M ratios for the DU145 and 22Rv1 (prostate) tumors were 6.7 ± 0.1 and 2.8 ± 0.2, respectively. Considerable de-iodination of [^{125}I]Axl mAb, probably due to internalization, was observed as indicated by the highest accumulation of radioactivity in the thyroid (data not shown).

The control [^{125}I]IgG$_1$ antibody showed uniform distribution of radioactivity both in tumors and normal organs with minimal variation in distribution over 120 h. Very low de-iodination of this antibody was observed (Supplementary Fig. 3).

4. Discussion

We report the preclinical evaluation of a radiolabeled antibody demonstrating the feasibility of imaging graded levels of Axl expression in both pancreatic and prostate tumors *in vivo*. Axl is overexpressed in cancer from a variety of tissues of origin. There is accumulating literature supporting the role of Axl in tumor growth, angiogenesis, metastasis and acquired resistance to therapy. The first low-molecular-weight inhibitor of Axl is in clinical trials, and humanized, monoclonal antibodies are in development to block Axl signaling in cancer [22]. Our studies suggest that Axl imaging may provide a new strategy for characterizing Axl-positive tissues *in vivo*, such as for selecting appropriate patients for anti-Axl therapy, staging and therapeutic monitoring.

Pancreatic cancer is one of the leading causes of cancer death in the United States with a median survival of less than six months and a five year survival rate that is <5% [25]. Pancreatic cancer is nearly undetectable in early stages, with few diagnostic options available. Previously we have shown that 55% of pancreatic cancers demonstrate overexpression of Axl [12], and now extend these observations with the development of a noninvasive tool that may aid in clinical staging and monitoring of pancreatic cancer.

Over the past decade immunoPET has been gaining attention in the detection and management of cancer [26]. This is particularly important for cell surface targets with few readily available

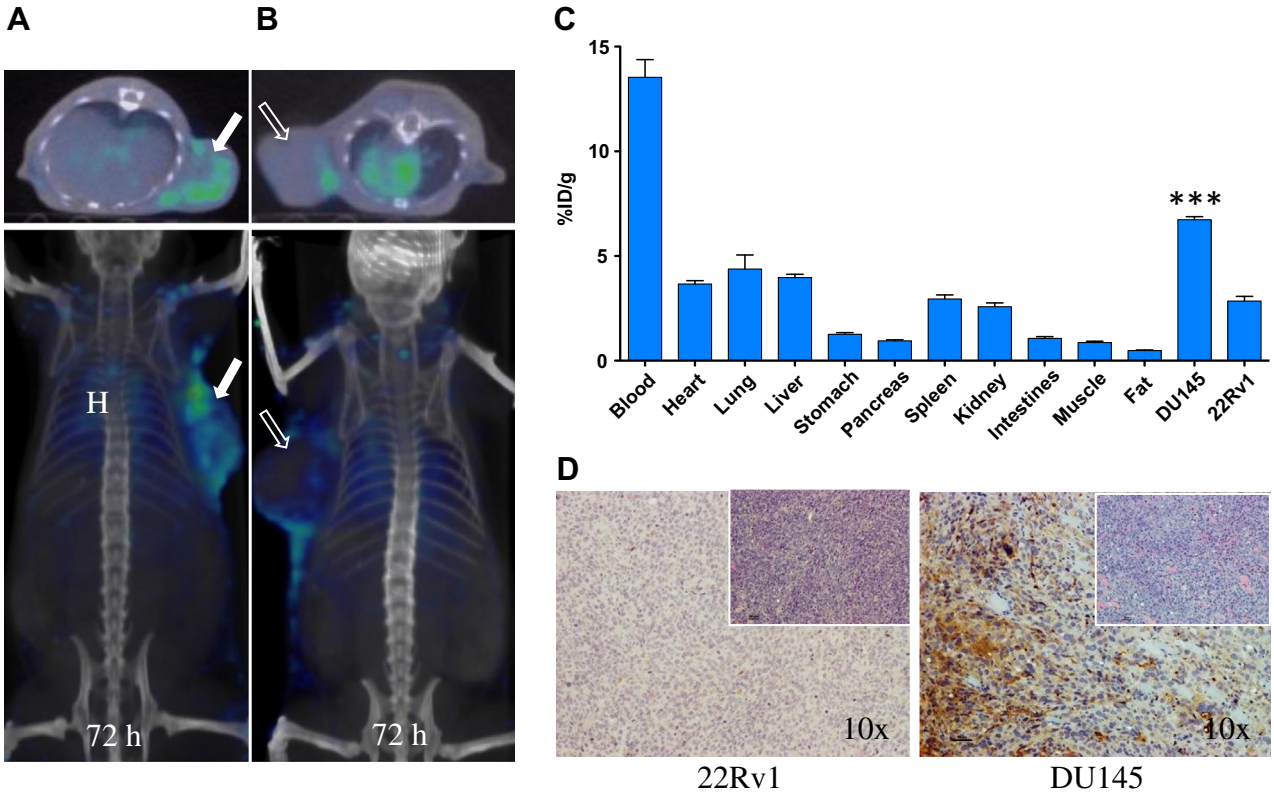

Fig. 4. SPECT/CT imaging and *ex vivo* biodistribution of [^{125}I]Axl mAb in prostate cancer xenografts. NOD/SCID mice bearing either 22Rv1 or DU145 prostate xenografts were given 0.75 mCi of [^{125}I]Axl mAb *via* tail vein injection. SPECT/CT images were acquired at 72 h after injection of the [^{125}I]Axl mAb. Representative transaxial and volume rendered images are shown; unfilled arrow, 22Rv1 tumor (A); filled arrow, DU145 tumor (B); H, heart. NOD/SCID mice harboring either DU145 or 22Rv1 xenografts were given 30–35 μCi of [^{125}I]Axl mAb *via* tail vein injection. At 72 h post-injection selected tissues and tumors were harvested, weighed and radioactivity was counted in gamma spectrometer. All the values were converted into percentage of injected dose per gram of tissue (%ID/g). Data are means ± SEM of three to four animals. The significance of the value is indicated by asterisks (∗) and the comparative reference is the uptake in the 22Rv1 tumor. $^{***}P < 0.001$ (C). Axl and hematoxylin and eosin (inset) staining of the 22Rv1 and DU145 xenografts at 10× magnification (D).

low-molecular-weight agents or peptide-based antagonists that are amenable for radiolabeling. Although several low-molecular-weight inhibitors have been generated that target Axl [27], they are highly hydrophobic, which can produce significant, unwanted non-specific binding in imaging studies, further prompting us to pursue immunoimaging as proof of principle for detection of this important target. In this study we demonstrated that [^{125}I]Axl mAb specifically bound to and accumulated within the Axl^{high} CFPAC xenografts compared to the Axl^{low} Panc1 tumors within the same mouse. The ability of the [^{125}I]Axl mAb to image graded levels of Axl expression was also confirmed in orthotopic pancreatic tumor xenografts. In the pancreatic tumor models, tumor uptake was closely associated with Axl expression as confirmed by immunohistochemistry, further supporting the utility of using radiolabeled antibodies as imaging agents. Although we have pursued radioiodination with ^{125}I, due to its ready availability, ease of introduction to antibodies and low expense, radiolabeling of these antibodies with more suitable radionuclides such as the long-lived, positron-emitting isotope, ^{89}Zr ($t_{1/2}$ 3.8 days), may minimize the continuous clearance of radioactivity we noted due to de-iodination of the Axl-targeted antibody. Furthermore, ^{89}Zr radiolabeling will allow for imaging at higher sensitivity and resolution as well as fully quantitative kinetic analysis, all of which are in the domain of positron emission tomography (PET) [28].

Prostate cancer is the second leading cause of cancer-related death in men in the United States [25]. Similar to pancreatic cancer, prostate cancer has few diagnostic options available, particularly to differentiate indolent from aggressive disease. Axl is also overexpressed in ~50% of prostate cancers [13,14]. Inhibition or blockade of Axl overexpression in prostate cancer cell lines inhibits proliferation, migration and invasion suggesting that Axl may contribute to the metastatic potential of prostate tumors [10,13,29]. Furthermore, phosphorylation of Axl leads to activation of the NF-kB pathway, which plays a critical role in cancer cell survival and metastasis [14]. In our studies [^{125}I]Axl mAb showed high accumulation in the metastatic and Axl^{high} DU145 tumors compared to the 22Rv1 Axl^{low} tumors. Although we have used subcutaneous tumor models, Axl specific accumulation supports the feasibility of imaging Axl in tumors that derive from a variety of tissues of origin. The DU145 cell line showed highest Axl expression of the cell lines tested and the highest binding and uptake of the [^{125}I]Axl mAb *in vitro*. However, the *in vivo* uptake in DU145 tumors, although higher than for 22Rv1 tumors, was not significantly different from that of pancreatic CFPAC tumors. High Axl expression led to increased vascularity, while inhibition of Axl reduced vessel density and diameter [15,16]. We speculate that changes in tumor vascular properties due to elevated Axl expression levels, although not validated in the current study, could contribute to accumulation of antibody within tumor [30]. Axl also exists in cleavable, soluble form and the concentration and variability of soluble Axl in tumors is not known [31]. Another possibility for differences in radiolabeled antibody uptake is that freely available soluble Axl within plasma may bind to the radiolabeled antibody and reduce the availability and accumulation of the radiolabeled antibody in the tumors [31]. Also, it is not known whether the antibody we have used for imaging also binds to the soluble

form of Axl. Further studies are warranted to investigate the role soluble Axl may play in imaging Axl expression in tumors.

In conclusion, we have imaged pancreatic and prostate tumors with graded levels of Axl expression, with the degree of radio-antibody uptake correlating with this expression. Because of the importance of Axl to invasion and metastasis, quantitative imaging of this target provides a new way to visualize and measure this important cancer target *in vivo*.

Acknowledgments

We would like to thank Dr. Akhilesh Pandey for helpful discussions. Work in Maitra, Nimmagadda and Pomper laboratories is partially supported by R01 CA113669 (AM), R01CA166131 (SN), R01CA138636 (MGP), P50 CA103175 (MGP), U54CA151838 (AM & MGP) and the Alexander and Margaret Stewart Trust (SN). This work is also supported by the resources provided through P30 CA006973, U54CA151838 and P50 CA103175.

Appendix A. Supplementary data

Supplementary data associated with this article can be found, in the online version, at http://dx.doi.org/10.1016/j.bbrc.2013.12.014.

References

[1] G. Lemke, Biology of the TAM Receptors, Cold Spring Harb. Perspect. Biol. 5 (11) (2013) 1–17.
[2] A. Verma, S.L. Warner, H. Vankayalapati, D.J. Bearss, S. Sharma, Targeting Axl and Mer kinases in cancer, Mol. Cancer Ther. 10 (10) (2011) 1763–1773.
[3] R.M. Linger, A.K. Keating, H.S. Earp, D.K. Graham, TAM receptor tyrosine kinases: biologic functions, signaling, and potential therapeutic targeting in human cancer, Adv. Cancer Res. 100 (2008) 35–83.
[4] T.N. Stitt, G. Conn, M. Gore, C. Lai, J. Bruno, C. Radziejewski, K. Mattsson, J. Fisher, D.R. Gies, P.F. Jones, et al., The anticoagulation factor protein S and its relative, Gas6, are ligands for the Tyro 3/Axl family of receptor tyrosine kinases, Cell 80 (4) (1995) 661–670.
[5] G. Berclaz, H.J. Altermatt, V. Rohrbach, I. Kieffer, E. Dreher, A.C. Andres, Estrogen dependent expression of the receptor tyrosine kinase axl in normal and malignant human breast, Ann. Oncol. 12 (6) (2001) 819–824.
[6] P. Dunne, D.G. McArt, J.K. Blayney, M. Kalimutho, S. Greer, T. Wang, S. Srivastava, C.W. Ong, K.J. Arthur, M. Loughrey, K. Redmond, D.B. Longley, M. Salto-Tellez, P.G. Johnston, S. Van Schaeybroeck, AXL is a key regulator of inherent and chemotherapy-induced invasion and predicts a poor clinical outcome in early stage colon cancer, Clin. Cancer Res. (2013), http://dx.doi.org/10.1158/1078-0432.CCR-13-1354.
[7] A. Hector, E.A. Montgomery, C. Karikari, M. Canto, K.B. Dunbar, J.S. Wang, G. Feldmann, S.M. Hong, M.C. Haffner, A.K. Meeker, S.J. Holland, J. Yu, T.J. Heckrodt, J. Zhang, P. Ding, D. Goff, et al., The Axl receptor tyrosine kinase is an adverse prognostic factor and a therapeutic target in esophageal adenocarcinoma, Cancer Biol. Ther. 10 (10) (2010) 1009–1018.
[8] M. Hutterer, P. Knyazev, A. Abate, M. Reschke, H. Maier, N. Stefanova, T. Knyazeva, V. Barbieri, M. Reindl, A. Muigg, H. Kostron, G. Stockhammer, A. Ullrich, Axl and growth arrest-specific gene 6 are frequently overexpressed in human gliomas and predict poor prognosis in patients with glioblastoma multiforme, Clin. Cancer Res. 14 (1) (2008) 130–138.
[9] L. He, J. Zhang, L. Jiang, C. Jin, Y. Zhao, G. Yang, L. Jia, Differential expression of Axl in hepatocellular carcinoma and correlation with tumor lymphatic metastasis, Mol. Carcinog. 49 (10) (2010) 882–891.
[10] R.M. Linger, R.A. Cohen, C.T. Cummings, S. Sather, J. Migdall-Wilson, D.H. Middleton, X. Lu, A.E. Baron, W.A. Franklin, D.T. Merrick, P. Jedlicka, D. DeRyckere, L.E. Heasley, D.K. Graham, Mer or Axl receptor tyrosine kinase inhibition promotes apoptosis, blocks growth and enhances chemosensitivity of human non-small cell lung cancer, Oncogene 32 (29) (2013) 3420–3431.
[11] T. Ito, M. Ito, S. Naito, A. Ohtsuru, Y. Nagayama, T. Kanematsu, S. Yamashita, I. Sekine, Expression of the Axl receptor tyrosine kinase in human thyroid carcinoma, Thyroid 9 (6) (1999) 563–567.
[12] J.B. Koorstra, C.A. Karikari, G. Feldmann, S. Bisht, P.L. Rojas, G.J. Offerhaus, H. Alvarez, A. Maitra, The Axl receptor tyrosine kinase confers an adverse prognostic influence in pancreatic cancer and represents a new therapeutic target, Cancer Biol. Ther. 8 (7) (2009) 618–626.
[13] Y. Shiozawa, E.A. Pedersen, L.R. Patel, A.M. Ziegler, A.M. Havens, Y. Jung, J. Wang, S. Zalucha, R.D. Loberg, K.J. Pienta, R.S. Taichman, GAS6/AXL axis regulates prostate cancer invasion, proliferation, and survival in the bone marrow niche, Neoplasia 12 (2) (2010) 116–127.
[14] J.D. Paccez, G.J. Vasques, R.G. Correa, J.F. Vasconcellos, K. Duncan, X. Gu, M. Bhasin, T.A. Libermann, L.F. Zerbini, The receptor tyrosine kinase Axl is an essential regulator of prostate cancer proliferation and tumor growth and represents a new therapeutic target, Oncogene 32 (6) (2013) 689–698.
[15] P. Vajkoczy, P. Knyazev, A. Kunkel, H.H. Capelle, S. Behrndt, H. von Tengg-Kobligk, F. Kiessling, U. Eichelsbacher, M. Essig, T.A. Read, R. Erber, A. Ullrich, Dominant-negative inhibition of the Axl receptor tyrosine kinase suppresses brain tumor cell growth and invasion and prolongs survival, Proc. Natl. Acad. Sci. USA 103 (15) (2006) 5799–5804.
[16] S.J. Holland, M.J. Powell, C. Franci, E.W. Chan, A.M. Friera, R.E. Atchison, J. McLaughlin, S.E. Swift, E.S. Pali, G. Yam, S. Wong, J. Lasaga, M.R. Shen, S. Yu, W. Xu, Y. Hitoshi, et al., Multiple roles for the receptor tyrosine kinase axl in tumor formation, Cancer Res. 65 (20) (2005) 9294–9303.
[17] Y.X. Zhang, P.G. Knyazev, Y.V. Cheburkin, K. Sharma, Y.P. Knyazev, L. Orfi, I. Szabadkai, H. Daub, G. Keri, A. Ullrich, AXL is a potential target for therapeutic intervention in breast cancer progression, Cancer Res. 68 (6) (2008) 1905–1915.
[18] Y. Li, X. Ye, C. Tan, J.A. Hongo, J. Zha, J. Liu, D. Kallop, M.J. Ludlam, L. Pei, Axl as a potential therapeutic target in cancer: role of Axl in tumor growth, metastasis and angiogenesis, Oncogene 28 (39) (2009) 3442–3455.
[19] R.M. Linger, A.K. Keating, H.S. Earp, D.K. Graham, Taking aim at Mer and Axl receptor tyrosine kinases as novel therapeutic targets in solid tumors, Expert Opin. Ther. Targets 14 (10) (2010) 1073–1090.
[20] X. Ye, Y. Li, S. Stawicki, S. Couto, J. Eastham-Anderson, D. Kallop, R. Weimer, Y. Wu, L. Pei, An anti-Axl monoclonal antibody attenuates xenograft tumor growth and enhances the effect of multiple anticancer therapies, Oncogene 29 (38) (2010) 5254–5264.
[21] L. Cerchia, C.L. Esposito, S. Camorani, A. Rienzo, L. Stasio, L. Insabato, A. Affuso, V. de Franciscis, Targeting Axl with an high-affinity inhibitory aptamer, Mol. Ther. 20 (12) (2012) 2291–2303.
[22] C. Sheridan, First Axl inhibitor enters clinical trials, Nat. Biotechnol. 31 (9) (2013) 775–776.
[23] S. Nimmagadda, M. Pullambhatla, M.G. Pomper, Immunoimaging of CXCR4 expression in brain tumor xenografts using SPECT/CT, J. Nucl. Med. 50 (7) (2009) 1124–1130.
[24] G. Feldmann, S. Dhara, V. Fendrich, D. Bedja, R. Beaty, M. Mullendore, C. Karikari, H. Alvarez, C. Iacobuzio-Donahue, A. Jimeno, K.L. Gabrielson, W. Matsui, A. Maitra, Blockade of hedgehog signaling inhibits pancreatic cancer invasion and metastases: a new paradigm for combination therapy in solid cancers, Cancer Res. 67 (5) (2007) 2187–2196.
[25] R. Siegel, D. Naishadham, A. Jemal, Cancer statistics, 2013, CA Cancer J. Clin. 63 (1) (2013) 11–30.
[26] S.M. Knowles, A.M. Wu, Advances in immuno-positron emission tomography: antibodies for molecular imaging in oncology, J. Clin. Oncol. 30 (31) (2012) 3884–3892.
[27] A. Mollard, S.L. Warner, L.T. Call, M.L. Wade, J.J. Bearss, A. Verma, S. Sharma, H. Vankayalapati, D.J. Bearss, Design, synthesis and biological evaluation of a Series of novel Axl kinase inhibitors, ACS Med. Chem. Lett. 2 (12) (2011) 907–912.
[28] M.A. Deri, B.M. Zeglis, L.C. Francesconi, J.S. Lewis, PET imaging with (8)(9)Zr: from radiochemistry to the clinic, Nucl. Med. Biol. 40 (1) (2013) 3–14.
[29] P.P. Sainaghi, L. Castello, L. Bergamasco, M. Galletti, P. Bellosta, G.C. Avanzi, Gas6 induces proliferation in prostate carcinoma cell lines expressing the Axl receptor, J. Cell Physiol. 204 (1) (2005) 36–44.
[30] H. Maeda, J. Wu, T. Sawa, Y. Matsumura, K. Hori, Tumor vascular permeability and the EPR effect in macromolecular therapeutics: a review, J. Controlled Release 65 (1–2) (2000) 271–284.
[31] J.P. O'Bryan, Y.W. Fridell, R. Koski, B. Varnum, E.T. Liu, The transforming receptor tyrosine kinase, Axl, is post-translationally regulated by proteolytic cleavage, J. Biol. Chem. 270 (2) (1995) 551–557.